MATERIALS SCIENCE

A breathable, biodegradable, antibacterial, and self-powered electronic skin based on all-nanofiber triboelectric nanogenerators

Xiao Peng[1,2]*, Kai Dong[1,2]*, Cuiying Ye[1,2], Yang Jiang[1,2], Siyuan Zhai[3], Renwei Cheng[1,2], Di Liu[1,2], Xiaoping Gao[4], Jie Wang[1,2]†, Zhong Lin Wang[1,2,5]†

Mimicking the comprehensive functions of human sensing via electronic skins (e-skins) is highly interesting for the development of human-machine interactions and artificial intelligences. Some e-skins with high sensitivity and stability were developed; however, little attention is paid to their comfortability, environmental friendliness, and antibacterial activity. Here, we report a breathable, biodegradable, and antibacterial e-skin based on all-nanofiber triboelectric nanogenerators, which is fabricated by sandwiching silver nanowire (Ag NW) between polylactic-co-glycolic acid (PLGA) and polyvinyl alcohol (PVA). With micro-to-nano hierarchical porous structure, the e-skin has high specific surface area for contact electrification and numerous capillary channels for thermal-moisture transfer. Through adjusting the concentration of Ag NW and the selection of PVA and PLGA, the antibacterial and biodegradable capability of e-skins can be tuned, respectively. Our e-skin can achieve real-time and self-powered monitoring of whole-body physiological signal and joint movement. This work provides a previously unexplored strategy for multifunctional e-skins with excellent practicability.

INTRODUCTION

As the largest organ of the body, human skin not only has the basic functions of protection, secretion, and respiration but also is an important somatosensory system for human to perceive, interact, and communicate with our physical world (*1*–*3*). Considerable interests have been stimulated to develop bioinspired e-skins by mimicking features and functionalities of natural skin that have broad applications in wearable individual-centered health monitoring (*4*–*6*), intelligent prostheses and robotics (*7*, *8*), human-machine interfaces (*9*–*11*), and artificial intelligences (*12*, *13*). On the basis of different physical sensing mechanisms, such as piezoresistivity, capacitance, piezoelectricity, and triboelectricity, e-skins are able to detect and quantify a diversity of environmental stimuli, including temperature, humidity, pressure, vibration, and haptics, through transforming them into real-time and visualized electronic impulses (*7*, *14*–*18*). In particular, triboelectric nanogenerator (TENG) is a newly developed energy-harvesting technology that can convert ubiquitous mechanical energy into precious electricity based on the coupling effect of contact electrification and electrostatic induction (*19*–*23*). With the advantages of low cost, simple structure, easy to access, diverse material option, and high conversion efficiency, TENG has a broad application potential in both wearable power supplying and self-powered sensing, making it a promising candidate for energy autonomous e-skins (*14*, *24*–*26*).

It is well known that flexibility, stretchability, sensitivity, ultraconformality, and mechanical durability are the most concerned and the most popular research directions of e-skins, which are also relatively easy to implement. Recently, aiming to improving the comprehensive performance of e-skins, special functionalities, such as recyclability (*3*), self-healing (*27*), shape memory (*28*), electroluminescence (*29*), and mechanoluminescence (*30*) are gradually added or integrated. Although the above aspects have been optimized and improved continuously, the comfort, safety, and health of e-skins are always neglected, which hinders their practical applications to a great extent. Therefore, the e-skins with desired comfortability and practicability must have the performance of breathability, biodegradability, and antibacterial activity. Breathability is an important means to adjust thermal-moisture balance and achieve gas exchange between the human body and the external environment (*31*, *32*). However, most high-performance e-skins take the membranes as electrodes or substrates, which may cause skin discomfort and even induce inflammation and itching. In addition, considering that e-skins are excellent media for microorganism growth due to prolonged contact with human skin or unhealthy indoor air quality, antibacterial characteristic is a vital performance optimization for e-skins to inhibit bacterial growth and prevent bacterial infections (*33*–*35*). Furthermore, the majority of materials are not disposable, which may become electronic wastes at the end of their service life period and even harm the human body or pollute the environment (*36*–*38*). Nontoxic biodegradable electronics that can function over the prescribed time frames and then fully degrade into nonharmful constitutes without any adverse long-term side effects would reduce electronic waste disposal and environmental impact. Therefore, the performance optimization and large-scale practical application of e-skins should take the breathability, biodegradability, and antibacterial activity into account.

Here, we designed a flexible, stretchable, breathable, biodegradable, and antibacterial e-skin on the basis of all-nanofiber TENGs for effective mechanical energy harvesting and whole-body physiological signal monitoring. By sandwiching the silver nanowire (Ag NW) electrode between the top polylactic-co-glycolic acid (PLGA) triboelectric

[1]Beijing Institute of Nanoenergy and Nanosystems, Chinese Academy of Sciences, Beijing 100083, P. R. China. [2]College of Nanoscience and Technology, University of Chinese Academy of Sciences, Beijing 100049, P. R. China. [3]Research Center for Eco-environmental Science, Chinese Academy of Sciences, Beijing, 100085, P. R. China. [4]College of Light Industry and Textile, Inner Mongolia University of Technology, Hohhot, 010051, P. R. China. [5]School of Materials Science and Engineering, Georgia Institute of Technology, Atlanta, GA 30332, USA.
*These authors contributed equally to this work.
†Corresponding author. Email: wangjie@binn.cas.cn (J.W.); zhong.wang@mse.gatech.edu (Z.L.W.)

layer and the bottom polyvinyl alcohol (PVA) substrate, the all-nanofiber TENG–based e-skin with multilayer interlaced nanofiber network and numerous three-dimensional micro-to-nano hierarchical pores provides high specific surface area for contact electrification and pressure sensing and multiple interfiber capillary channels for thermal-moisture transfer. The e-skin exhibits remarkable antibacterial activity against *Escherichia coli* and *Staphylococcus aureus*, which can effectively inhibit bacterial growth and prevent bacterial infections. In addition, the e-skin can regulate its service life period from hours to weeks through the selection and collocation of degradable PLGA and PVA. With the maximum peak power density of 130 mW m^{-2} and the voltage response pressure sensitivity of 0.011 kPa^{-1}, the all-nanofiber TENG–based e-skin is able to realize the whole-body monitoring of physiological signal (e.g., microexpression, pulse, respiration, and vocalization) and joint movement (e.g., knuckle, elbow, knee, and ankle) in a real-time, noninvasive, and self-powered manner. Our work presents a comfortable, safe, and pollution-free e-skin with energy-harvesting and highly sensitive capability by integrating breathability, biodegradability, and antibacterial activity, which helps to promote more practical and environmentally friendly applications of e-skins in human-machine interface and artificial intelligence.

RESULTS

Structural design and composition characterization of all-nanofiber TENG–based e-skin

As conceptually shown in Fig. 1A, the all-nanofiber TENG–based e-skin that integrates breathability, biodegradability, and antibacterial activity can be conveniently and conformally attached onto the epidermis. The e-skin consists of three functional layers, including the top PLGA for contact electrification and water proofing, the middle Ag NWs for conducting electrode and antibacterial agent, and the bottom PVA for flexible substrate and skin contact (Fig. 1B). According to the structural sequence, the e-skin is represented as the top layer/middle layer/down layer, for example, PLGA/Ag NWs/PVA. The fabrication procedures of the e-skin are illustrated in fig. S1, which are further described in Materials and Methods in detail. Both PLGA and PVA nanofiber networks are prepared via a facile electrospinning strategy. Fourier transform infrared (FTIR) spectra of PLGA and PVA nanofibers indicate that their chemical compositions and structural characteristics will not change after electrospinning (fig. S2). The hydrophobic PLGA with contact angle of 115° can effectively prevent water from diffusing to the electrode, whereas the hydrophilic PVA (contact angle, 38°) as a wicking layer can rapidly absorb heat and sweat from the body and timely diffuse to the outside. As displayed in fig. S3, the red water drops are well suspended on the PLGA surface while rapidly diffused to the surrounding on the PVA nanofiber film. Ag NWs with an average diameter of 167 nm (fig. S4) are tangled together to form a continuous percolated network (lower right in Fig. 1B) on the top of the PVA nanofibers, which provide a continuous electron transport pathway with high conductivity and good mechanical flexibility. Numerous three-dimensional micro-to-nano hierarchical pores constructed by the multilayer stacking nanofiber networks endow the e-skin with high flexibility, appropriate stretchability, large specific surface area, outstanding breathability, and high structural stability. In addition, gas and water molecules can easily pass through interfiber capillary channels to adjust the thermal-moisture equilibrium of the microenvironment between human skin and outer environment.

The microstructural morphologies and diameter distributions of the PLGA and PVA nanofibers are optimized through adjusting the electrospinning parameters, such as solution concentrations, applied voltages, flow rates, and receiving distances (figs. S5 to S10). The optimum electrospinning conditions for the PLGA nanofibers are 8.5 weight % (wt %), 15 kV, and 0.45 ml/hour, and those for the PVA nanofibers are 10 wt %, 25 kV, and 0.5 ml/hour. The surface morphologies of the optimized PLGA and PVA nanofibers observed by scanning electron microscopy (SEM) are shown in Fig. 1 (C and D), in which their corresponding average fiber diameters are 600 and 130 nm. The photographs of the prepared all-nanofiber e-skin are exhibited in Fig. 1E, indicating that it is ultralight (80 mg) and rather thin (120 μm) and can be conformally wound on complex curved surfaces and even be stretched to 100% strain level. The disordered interconnected nanofiber networks can be gradually oriented along the direction of external loads, providing good stretchability and excellent deformability for the e-skin. X-ray diffraction (XRD) analysis on different nanofiber films confirm that the Ag element in Ag NWs is not oxidized during long-term use (Fig. 1F). In addition, the excellent oxidation resistance of Ag NWs is further verified after prolonged exposure to air and even a period of respiratory operation (fig. S11 and note S1). The cross-sectional (Fig. 1G) and surface (Fig. 1H) SEM images and corresponding energy-dispersive x-ray spectrometry (EDX) elemental mappings of the all-nanofiber e-skin confirm that the Ag NW electrode is sandwiched between the top PLGA triboelectric layer and the bottom PVA substrate. In addition, uniform elemental distribution, continuous conductive network, and surface undulating texture can be also observed from these images. The fluctuation degree of nanofibers is characterized by atomic force microscopy (AFM), showing that there are obvious height gradients at the location of nanofibers (fig. S12). Because of the addition of Ag NWs, the thermal stability of the e-skin is also greatly improved compared with pure PLGA and PVA nanofiber films (fig. S13).

Stretchability, breathability, and electrical output performance

For electronics in direct contact with skin, the first concern is their wearability and comfortability, which mainly involve flexibility, stretchability, and air and moisture permeability. In addition to the excellent flexibility, as described above, the tensile properties of different nanofiber films are also evaluated by uniaxial tensile tests (fig. S14). Both the tensile strength and toughness of PLGA are higher than those of PVA, making it more suitable for surface packaging (Fig. 2A). The interface adhesion between Ag NWs and PVA nanofibers is helpful to improve the tensile strength of the Ag NWs/PVA nanofiber film. The asynchronous tensile fracture between PLGA and PVA results in the progressive failure behavior of the composite nanofiber film, leading to the degradation of mechanical properties of e-skins. However, the e-skin can meet the requirement of actual application, considering that the maximum strain tolerance of human arm skin is about 27%. In addition, the tensile capability of the e-skin can be further improved by choosing PLGA as both the triboelectric layer and the substrate. The electrode resistance of our e-skins at different tensile strain levels is measured (figs. S15 and S16) and further discussed (note S2). With the increase in tensile strain, the percolation network of Ag NWs is first oriented along

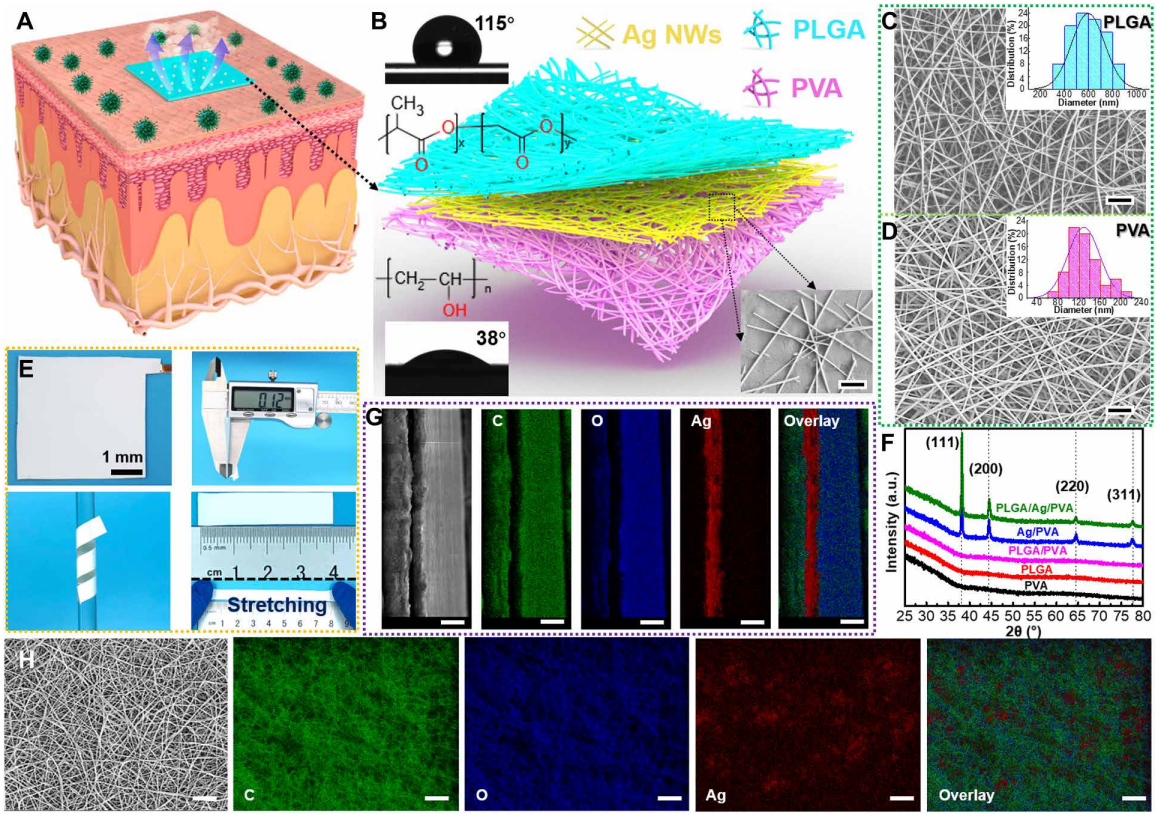

Fig. 1. Structural design and composition characterization of the all-nanofiber TENG–based e-skin. (**A**) Application scenario of the breathable, biodegradable, and antibacterial e-skin that can be conveniently and conformally attached onto the epidermis. (**B**) Schematic illustration of the three-dimensional network structure of the all-nanofiber TENG–based e-skin. The images of the water contact angle and molecular structure of PLGA and PVA are inserted on the top left and lower left, respectively. The surface scanning electron microscopy (SEM) image of the Ag NW electrode is inserted on the lower right (scale bar, 2 μm). (**C** and **D**) Optimized surface morphology SEM images of (C) PLGA (scale bar, 10 μm) and (D) PVA (scale bar, 2 μm) nanofiber films, in which their respective diameter distributions are shown in the upper right. (**E**) Photograph images of the e-skin with total thickness of 120 μm that can be wound onto a glass rod and stretched to 100% strain level. (**F**) Comparison of x-ray diffraction (XRD) profile among different nanofiber films. a.u., arbitrary units. (**G**) Cross-sectional (scale bars, 50 μm) and (**H**) surface morphology (scale bars, 20 μm) SEM images of the all-nanofiber TENG–based e-skin with energy-dispersive x-ray spectrometry (EDX) elemental mappings. Photo credit: X.P., Beijing Institute of Nanoenergy and Nanosystems.

the stretching direction, then separated from each other, and lastly blocked with the fracture of the device (fig. S17). Therefore, the higher the tensile strain level is, the more obvious the increase in electrode resistance will be. Breathability represents the property of fabric to exchange air and moisture between skin and environment, which plays a vital role in regulating and maintaining the temperature and humidity balance of human surface microenvironment. The air permeabilities of different nanofiber films are also measured (fig. S18). There are numerous micro/nanopores in the multilayer stacked nanofiber network, making it easy for gas and water molecules to transport through interfiber channels. Although the addition of Ag NWs leads to the air permeability of e-skin lower than that of its single components even under the same thickness (Fig. 2B), the breathability of e-skin (~120 mm s^{-1}) is still far higher than that of commercial jeans (~10 mm s^{-1}). In addition, the air permeability of e-skin decreases with the increase in nanofiber film thickness (Fig. 2B) but improves with the increase in pressure difference (Fig. 2C). Moreover, the increase in ambient humidity will weaken the air permeability of e-skin, which is due to that the dimensional swelling of fiber caused by moisture absorption leads to the reduction in porosity and part of the water will block the passage (fig. S19). Nevertheless, the air permeability remains 40 mm s^{-1} at the relative humidity of 80%. The microenvironment established between skin and environment is composed of numerous micro-to-nano hierarchical pores and crisscrossed interfiber channels, which can exchange and balance gas and water molecules timely, dynamically, and reversibly according to the internal and external conditions so as to achieve the thermal-moisture comfort of the human body (inserted in Fig. 2C). Here, the thermal-moisture stability and comfortability of the all-nanofiber e-skin are further discussed in note S3.

Our all-nanofiber TENG–based e-skin will operate in a single-electrode mode when the inner Ag NW electrode is grounded through external resistance. The electricity generation and transmission mechanism of the TENG-based e-skin are illustrated in fig. S20, which is realized by the periodic contact and separation movements between the e-skin and its contact object. The induced potential difference between the inner electrode and the ground will cause charge transfer between them and then generate an instantaneous current. As a result, a contact-separation process between the e-skin and the contact object will generate an alternating potential and current through external loads. The detailed explanations of

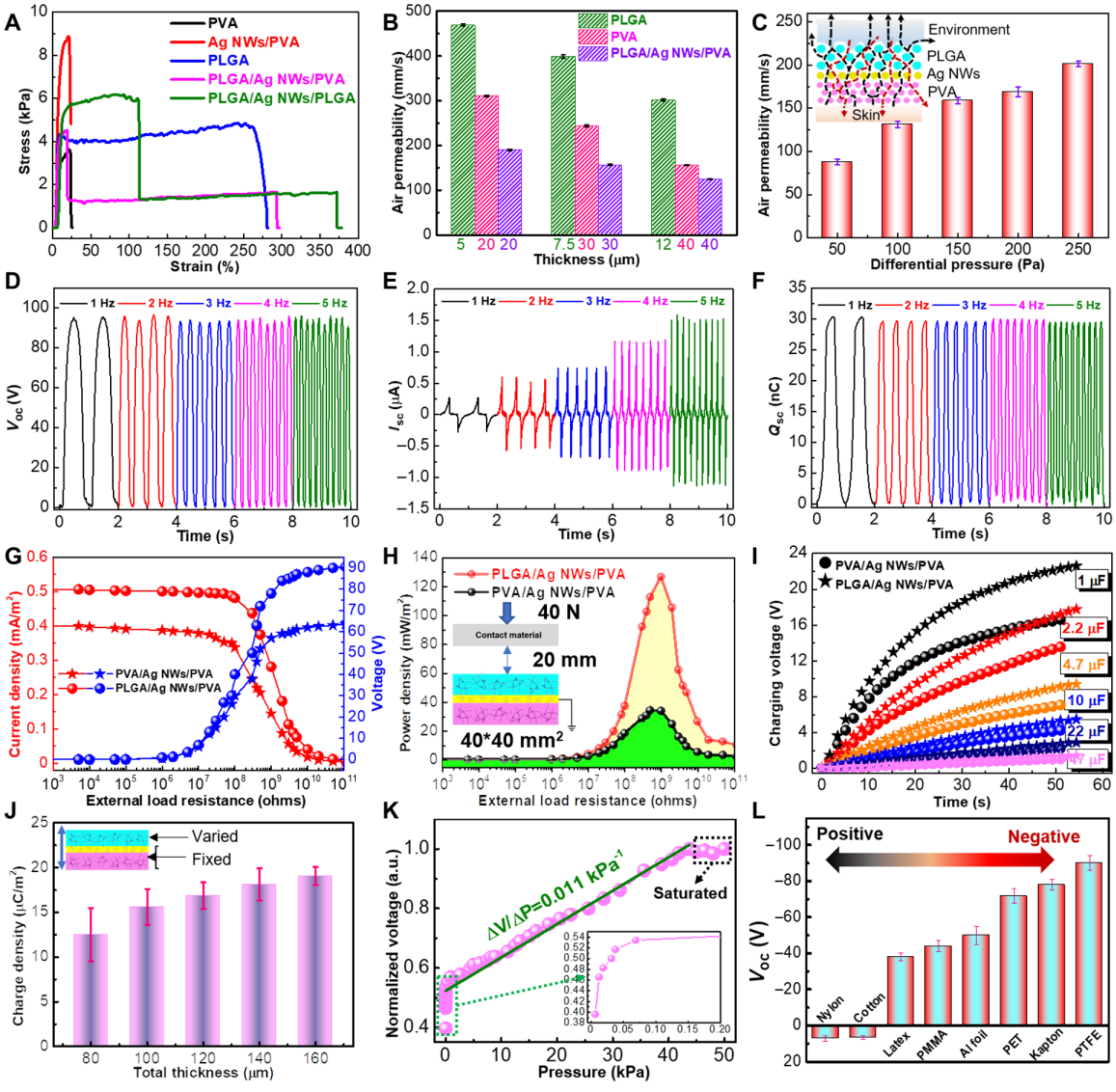

Fig. 2. Stretchability, breathability, and electrical output performance. (**A**) Uniaxial tensile stress-strain behaviors of PVA, Ag NWs/PVA, PLGA, PLGA/Ag NWs/PVA, and PLGA/Ag NWs/PLGA nanofiber films. (**B**) Thickness dependence of the air permeability of PVA, PLGA, and PLGA/Ag NWs/PVA nanofiber films. (**C**) Differential pressure response to the air permeability of PLGA/Ag NWs/PVA nanofiber films. The diagram of the air and moisture flow directions in the microenvironment between human skin and outer environment is inserted. (**D** to **F**) Frequency-response characteristics of the PLGA/Ag NWs/PVA e-skin, including (D) V_{OC}, (E) I_{SC}, and (F) Q_{SC}. (**G** and **H**) Comparison of (G) output voltage and current density, as well as (H) peak power density between the PLGA/Ag NWs/PVA and the PVA/Ag NWs/PVA e-skins under varied external resistances. (**I**) Analysis of charging performance between the two e-skins under different capacitance capacities. (**J**) Thickness-dependent charge output densities of the e-skin. Only the thickness of PLGA is varied, while that of Ag NWs/PVA is fixed. (**K**) Normalized output voltage response to a wide range of pressure. (**L**) Voltage response of the e-skin with relative contact-separation motion to different materials.

the working mechanism of the e-skin are conducted in note S4. In addition, a finite element analysis was established by using COMSOL Multiphysics to observe the potential distribution of every component in the e-skin from full contact to complete separation (fig. S21). The electrical output capability of TENGs is often reflected by the open-circuit voltage (V_{OC}), short-circuit current (I_{SC}), and charge transfer (Q_{SC}). The corresponding electrical outputs of the two kinds of e-skins (PLGA/Ag NWs/PVA and PVA/Ag NWs/PVA) were measured with polytetrafluoroethylene (PTFE) film (0.1-mm thickness) as the contact material under the loading frequencies from 1 to 5 Hz (Fig. 2, D to F, and fig. S22). It is found that the V_{OC} and Q_{SC} are approximately stable, but the I_{SC} presents a growth trend. The inconsistent variation of electrical output characteristics with loading frequency is explained in fig. S23 and note S5 (*39*). Taking PTFE film as the counter friction layer, PLGA/Ag NWs/PVA e-skin has slightly higher electrical output than PVA/Ag NWs/PVA e-skin, which can be attributed to the higher electron transfer quantity of PLGA than that of PVA (note S6) (*40*, *41*). At the applied frequency of 3 Hz, the electrical output performance of our e-skins is further measured by connecting varied external resistances in series. As the value of resistance increases, the current density tends to decrease, but the voltage shows an upward trend, which is ruled

by Ohm's law (Fig. 2G). Moreover, the voltage and current output of the PLGA/Ag NWs/PVA e-skin are higher than those of the PVA/Ag NWs/PVA e-skin within the whole resistance range. The power density was calculated as

$$P = I^2 R/A \quad (1)$$

where I is the output current under the corresponding resistance R, and A is the effective contact area. The maximum areal power density of the PLGA/Ag NWs/PVA e-skin is ~130 mW m^{-2} at a matched resistance of ~500 megohms, which is four times more than that of the PVA/Ag NWs/PVA e-skin (Fig. 2H). The charging capability of the e-skins to different commercial capacitors is also analyzed and compared (Fig. 2I). The result shows that charging speeds accelerate with the increase in capacitances. For example, the voltage of the 1-μF capacitor can reach 22 V, while that of the 47-μF capacitor is only 2 V after charging for 50 s. Moreover, the charging ability of the PVA/Ag NWs/PVA e-skin is obviously weaker than that of the PLGA/Ag NWs/PVA e-skin at the same charging time. The remarkable power output ability of the e-skin makes it a promising candidate in the field of wearable power supply and self-powered sensors in the future.

The impact of nanofiber film thickness on the electricity-generating capability of e-skin is also discussed (Fig. 2J). It is worth noting that only the thickness of the PLGA triboelectric layer is varied, whereas those of the PVA substrate and the Ag NW electrode are fixed. The increase in triboelectric layer thickness is not only beneficial to fully contact with outer objects but also can reduce the charge leakage caused by electrode exposure. The pressure sensitivity of our e-skin is measured over a large pressure range (Fig. 2K). The pressure sensitivity of the e-skin is defined as the slope of normalized voltage versus pressure curve, i.e.

$$S = d(\Delta V/V_S)/dP_F \quad (2)$$

where ΔV is the relative change in voltage, V_S is the saturation voltage, and P_F is the applied pressure. The e-skin exhibits almost a linear relationship within a pressure of 40 kPa, with a voltage response pressure sensitivity of 0.011 kPa^{-1}. The contact electrification ability of our e-skin response to different contact materials is also investigated. The amplitude and polarization of V_{OC} depend on the relative ability of a material to lose or gain electrons when contacting with the e-skin. Compared with PLGA, all the latex, polymethyl methacrylate, aluminum (Al), polyethylene terephthalate (PET), kapton, and PTFE are tending to gain electrons and, therefore, are more tribo-negative, whereas nylon and cotton are more tribo-positive (Fig. 2L). The larger the difference in the ability of losing/gaining electrons between two contacting materials, the more electrostatic charges generate at the interface and thus the higher output V_{OC}. Moreover, the mechanical durability of the e-skin was verified for 50,000 cycles of repeated loading-unloading under the pressure of 40 N and the frequency of 3 Hz (fig. S24). The voltage profile displays no noticeable fluctuation during the repetitive pushing tests, confirming that the performance of our e-skin is stable for long-term service.

Antibacterial and biodegradable test

On account of the e-skin being placed directly on the upper epidermis of the human body, its antimicrobial activity is extremely important. Silver exhibits a broad-spectrum biocidal property against specific bacteria, fungi, and viruses, making it the most promising antimicrobial agent for a wide range of medical application. Here, the antibacterial activities of the all-nanofiber TENG–based e-skins against two typical bacteria, i.e., gram-negative *E. coli* and gram-positive *S. aureus* (fig. S25), were determined by the commonly used zone of inhibition and colony count methods. For the zone of inhibition method, the diameter of the bacteriostatic zone represents the antibacterial ability. The diameters of the zone of inhibition against *E. coli* and *S. aureus* for the PLGA/Ag NWs/PVA nanofiber film were 10 and 12 mm, respectively, whereas the pure PVA and PLGA nanofiber films with an initial diameter of 8 mm show no antibacterial properties against both bacteria (Fig. 3, A and C, and fig. S26). The colony count method is further adopted to investigate the bactericidal efficacy of samples through the concentration of the survival colony bacteria in solution. After 24-hour incubation, the residual colonies for both *E. coli* and *S. aureus* on the agar petri dish are obviously less than the original (Fig. 3B). In addition, the bactericidal efficacy or killing efficiency for *E. coli* and *S. aureus* achieves up to 54 and 88%, respectively (Fig. 3C). The results from the zone of inhibition and colony count experiments indicate that our e-skin with Ag NW electrode has good antibacterial performance. It should be noted that antimicrobial properties can be improved gradually with the increase in Ag NW additive amount. The main antibacterial mechanism of our e-skin involves the release of silver ions that change the respiration or permeability of cell films, then penetrate into the bacteria, and continue to destroy by possibly interacting with the thiol groups of cellular proteins (*42*, *43*).

Biodegradation is another major property of our e-skin, which enables it to function over prescribed time frames and then physically degrade into nonharmful constituents. PLGA and PVA are well-known synthetic biodegradable materials, which can decompose over a period of time. For comparison purpose, the in vitro biodegradation tests of several types of nanofiber films were studied for 50 days, including PVA, PLGA, Ag NWs/PVA, PVA/Ag NWs/PVA, and PLGA/Ag NWs/PVA. The variations of their photographs and weight loss under corresponding degradation periods were recorded (Fig. 3, D and E, and fig. S27). The results showed that PVA presented rapid autocatalytic hydrolysis and bulk degradation after 3 days of incubation, whose weight loss was up to 90%. Moreover, it almost completely disappeared after 30 days of degradation. In contrast, the degradation cycle of the Ag NWs/PVA nanofiber film was slightly longer, because the existence of Ag NWs improved the impregnation resistance. The degradation morphologies and weight loss of the Ag NWs/PVA and PVA/Ag NWs/PVA nanofiber films were highly similar, which further verified the rapid hydrolysis ability of PVA. In contrary to PVA, PLGA has a strong resistance to weight loss and water absorption in the initial stage (0 to 21 days), but slightly shrinks and curls due to hydrolytic cleavage of the polymer backbone (fig. S28) (*40*, *44*). However, the degradation process of PLGA will be greatly accelerated after incubation over 30 days. Concurrently, crack appears on the surface of the PLGA nanofiber film and its density increases as the degradation time continues (Fig. 3F and fig. S28). In addition, the degradation time of our e-skin is adjustable based on the thickness of the PLGA or PVA film (fig. S29). Under the same thicknesses of the PLGA film and Ag NW layer, the weight loss of the PLGA/Ag NWs/PVA film increases with the increase in PVA film thickness. However, for the fixed thickness of the Ag NWs/PVA layer, the weight loss of the PLGA/Ag NWs/PVA film decreases first (before degradation of 21 days)

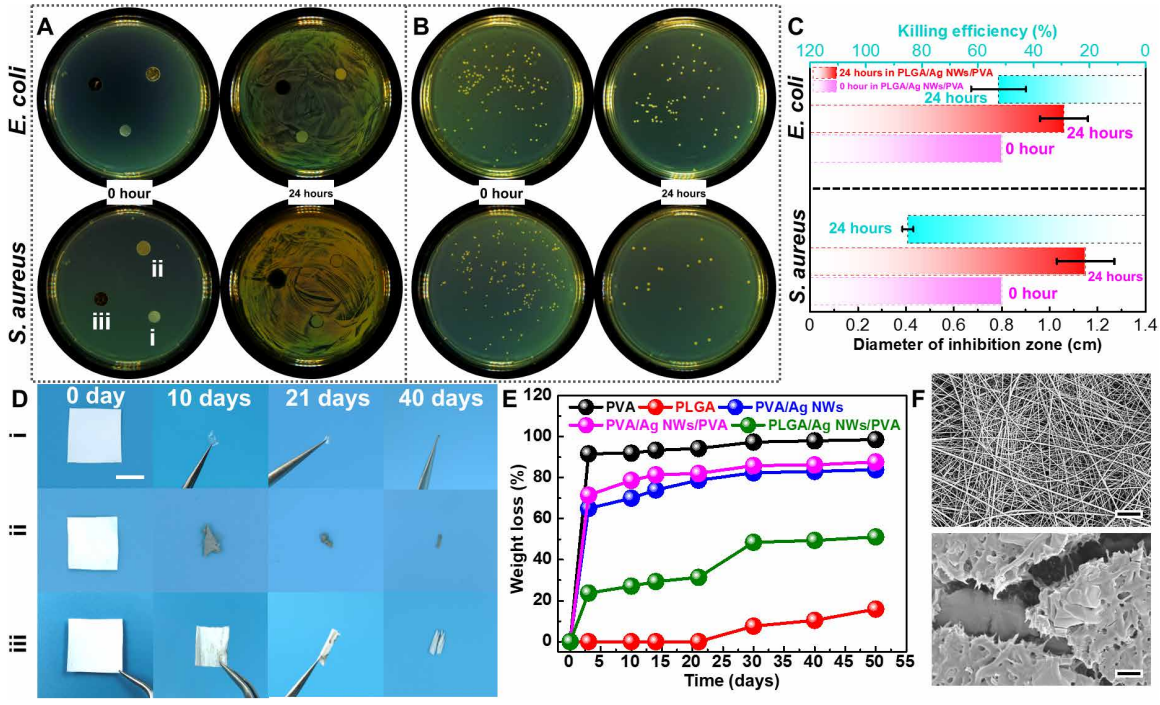

Fig. 3. Antibacterial activity and biodegradation process. (**A**) Photographs of inhibition zone of (i) PVA, (ii) PLGA, and (iii) PLGA/Ag NWs/PVA nanofiber films before (left) and after (right) 24-hour incubation. (**B**) Photographs of colonies of *S. aureus* and *E. coli* before and after coculturing for 24 hours. (**C**) Diameter of inhibition zone and antibacterial efficiency of the PLGA/Ag NWs/PVA nanofiber film after 24-hour incubation. (**D**) Sequential photographs of in vitro biodegradation of (i) PVA, (ii) Ag NWs/PVA, and (iii) PLGA/Ag NWs/PVA nanofiber films in phosphate-buffered saline (PBS) solutions (scale bar, 1 cm). (**E**) Weight loss rates of different nanofiber films within the degradation period of 50 days. (**F**) Surface morphology SEM images of the PLGA nanofiber film before (top) and after (bottom) the 50-day degradation (scale bars, 5 μm). Photo credit: X.P., Beijing Institute of Nanoenergy and Nanosystems.

and then increases with the increase in PLGA film thickness. The detailed discussion is presented in note S7. Combining the rapid degradation of PVA and the slow degradation of PLGA, the PLGA/Ag NWs/PVA shows moderate biodegradability. Although this unsynchronized degradation process may weaken the service performance of our e-skin, it can be well tuned by selecting the same materials as both the triboelectric layer and the substrate. Please note that although human sweat will weaken the electrical output ability of our e-skin (fig. S30), the PVA film can keep its structure stable without deformation, contraction, dissolution, or damage even at the maximum amount of human sweat (fig. S31) (*45*). It is also worth noting that the biodegradation of our e-skin has a notable negative impact on its electrical output performance, and the decline trend is more obvious as the degradation time continues (fig. S32), which can help us to better play the functions of our e-skin by mastering its gradual power attenuation ability.

Whole-body physiological and motion monitoring

The human body is a multisensory system with unique physiological signal characteristics for different parts. On the basis of the excellent pressure sensitivity and conformal ability, our e-skins are able to monitor various forms of human physiological signals for medical diagnosis and disease prevention in a rapid, real-time, noninvasive, and user-interactive way. Considering that a conformal and intimate contact between the e-skin and the human skin is paramount for subtle monitoring, the e-skins are conformally attached on the corresponding body parts with the aid of biocompatible medical bandages (Fig. 4A). All of these physiological data may have great clinical significance in modern medical diagnosis. Frowning, blinking, smiling, and other facial expressions are the most intuitive platforms to convey human emotions and are also the main external communication channels for general paralyzed patients. By sticking an e-skin on the forehead, regular and repeatable voltage signals are monitored during normal and frown alternating movements (Fig. 4B). Tiny muscle movements caused by microexpression can be easily captured by the voltage signal variations. Subtle voltage signals induced by blinking can also be collected by mounting an e-skin on the eyelid (Fig. 4C). Moreover, the differences of frequency and amplitude between normal blinking and rapid blinking can also be distinguished. Respiration is a primary vital sign that helps to assess health conditions, such as sleep quality and mood change, which can be reflected by the flow of breath, or the expansion and contraction of the chest and abdomen during inhalation and exhalation (*46*). To detect the flow of breath, the e-skin was placed on the vent of a conventional mask that could respond to the voltage signal changes during repeated oral breathing (Fig. 4D). Typically, one complete breathing cycle involves inhalation and exhalation, which generates an ascending and a descending voltage signal, respectively. More comprehensive respiratory information was obtained by situating the e-skin at the part of the chest or abdomen. The repeatable respiratory pattern from the abdomen was recorded with four distinctive breathing states including normal (shallow), slow, rapid, and deep (Fig. 4E).

The heart rate or pulse is often used as one of the critical vital signs to assess the physical and mental state of a person, which can

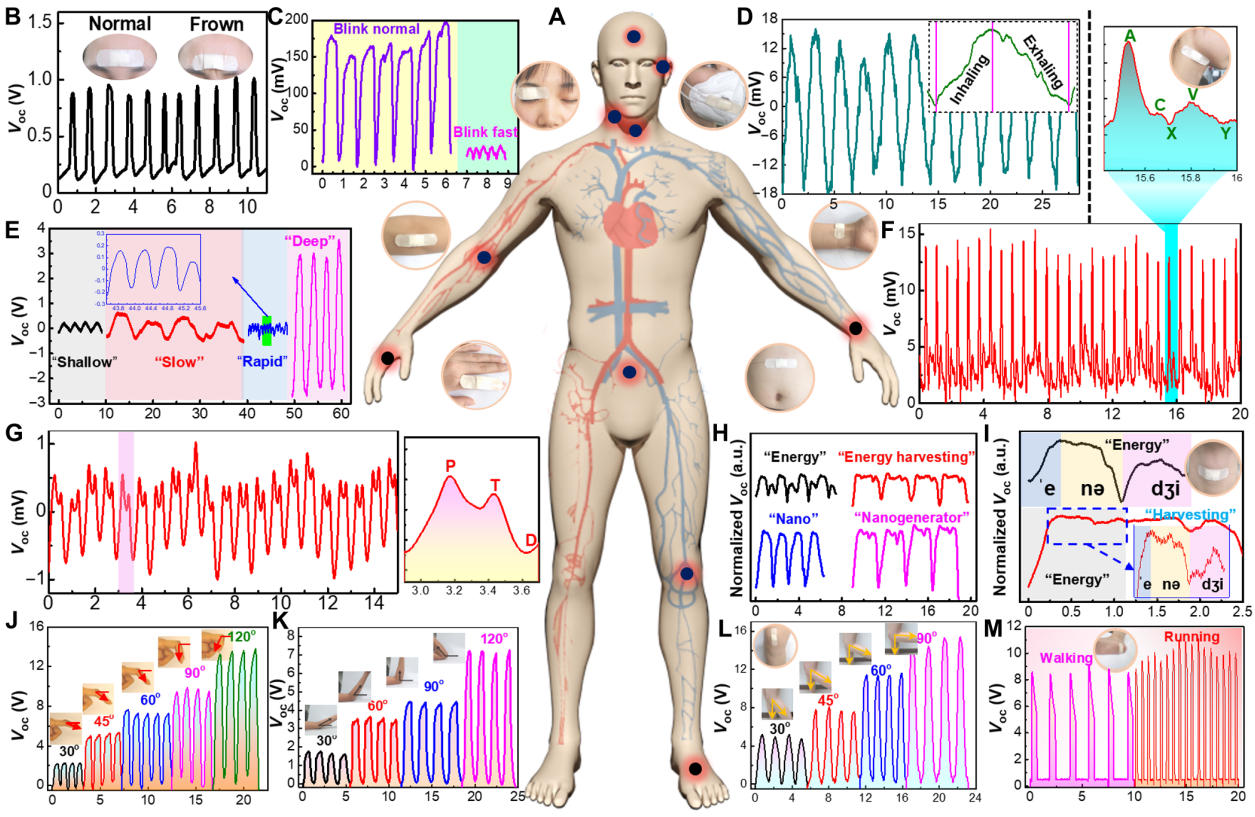

Fig. 4. Whole-body monitoring of physiological signal and joint movement. (**A**) Schematic illustration of a human body model with the detected parts marked with black solid circles. The photographs of corresponding detection parts in human body are also inserted. (**B**) Voltage response to the frown movement by attaching an e-skin on the forehead. (**C**) Monitoring of blinking behaviors by attaching an e-skin on the eyelid. (**D**) Normal oral breathing state monitoring by integrating an e-skin on a dust mask. The voltage signal during a single cycle of inhaling and exhaling is inserted. (**E**) Abdominal respiratory monitoring by pasting an e-skin on the human belly, including shallow (normal), slow, rapid, and deep. (**F**) Generated voltage signals in response to the jugular venous pulse (JVP) from the neck. A complete waveform is enlarged in the upper right. (**G**) Real-time monitoring of the radial artery pulse by attaching an e-skin to the wrist. The right enlarged is one complete radial artery pulse waveform containing "P," "T," and "D" peaks. (**H**) Sound and speech pattern recognition by mounting an e-skin on a volunteer's throat to detect his vocal cord vibrations. (**I**) Enlarged voltage signals from (H) for the analysis of repeatability, continuity, and stability. The regions marked with blue, yellow, and pink represent the voltage signals generated by the pronunciation of "ˈe," "nə," and "dʒi," respectively. (**J**) Detection of the finger bending angles by attaching an e-skin to the knuckle. (**K**) Detection of the arm flexion by attaching an e-skin to the elbow. (**L**) Detection of the leg swing angles by attaching an e-skin to the knee. (**M**) Detection of the foot movement states by fixing an e-skin on the heel. Note that all units of the abscissa are times. Photo credit: X.P., Beijing Institute of Nanoenergy and Nanosystems.

be measured from the radial artery at the wrist or from the carotid artery at the neck. The real-time radial artery pulse signals with regular and repeatable shape are recorded in 15 s by the e-skin when it is attached to a wrist as a pulse detector, indicating the frequency of 84 beats/min (Fig. 4G). In addition, a typical wrist pulse waveform is extracted with three characteristic peaks containing "P" (percussion wave), "T" (tidal wave), and "D" (diastolic wave), which are related to the systolic and diastolic blood pressure, the ventricular pressure, and the heart rate (*47*). In comparison to the radial artery pulse, the jugular venous pulse (JVP) can provide more valuable information for diagnosing heart diseases. As shown in Fig. 4F, the pulse frequency of the subject is 87 beats/min, which is consistent with the result of the radial artery pulse test. Similarly, a typical JVP waveform comprises three characteristic peaks, i.e., "A" (atrial systole), "C" (tricuspid bulging), and "V" (systolic filling of the atrium), and two descents, i.e., "X" (atrial relaxation) and "Y" (early ventricular filling) (*48*). The pulse frequency detected from the radial artery and JVP match well with those of normal adults. Voice recognition was achieved by conformally attaching the e-skin onto the throat to distinguish different words or phrases, such as "energy," "energy harvesting," "nano," and "nanogenerator" (Fig. 4H). Each word was recorded four times, and similar voltage signal characteristics for each curve can be seen, indicating the good repeatability for voice recognition. In addition, good consistency of voltage signal characteristics can be maintained between a word and its extended phrases (Fig. 4I and fig. S33). The ability of voice recognition might be useful for people with damaged vocal cords to rehabilitate their speech ability by training to control their throat muscle movement, which can also promote the implementation of remote human-machine interaction and control (*49*).

Our e-skin not only exhibits a remarkable response to the above subtle skin-level detections but can also track small bending movements of major joints, such as the knuckle, elbow, knee, and ankle. For example, the e-skin was fixed on the lateral knuckle of the index finger to record the voltage response under the bending-releasing cycles, with the bending angle from 30° to 120° (Fig. 4J). Similar motion angle detections of the elbow (Fig. 4K) and the knee (Fig. 4L) were realized by adhering the e-skins on corresponding joints (bent and

straightened to varying degrees). The voltage signals exhibit superior reproducibility under a certain joint bending angle, which confirms the excellent working stability and reliability of the e-skins. The slight difference in the output frequency of voltage signals is due to the inconsistency of the motion behaviors. The increase in voltage outputs at a large bending angle is attributed to the increase in contact area between the e-skin and the joints. The recognition and control of joint motion angle are helpful to realize the real-time and remote operation of robot movement, which, in turn, promotes the development of human-machine interaction and artificial intelligence. The human movement state is an important index to evaluate exercise intensity, which can be monitored by installing the e-skin on the ankle. As shown in Fig. 4M, there are notable differences in the amplitude and frequency of the generated voltage signals, which can well distinguish walking from running. From these demonstrations, it can be found that various physiological characteristics and movement behaviors can be transformed into readable, quantized, and real-time voltage signals through our e-skins, which is beneficial to realize parallel and whole-body physiological and motion monitoring. Therefore, it is expected that our e-skins will have promising applications in the fields of personal health monitoring, rehabilitation of patients, athletic performance monitoring, and human motion tracing for entertainments.

DISCUSSION

The seamless integration of excellent electrical responses and diversified practical functions is a major breakthrough in the development of e-skins. Here, a flexible, stretchable, conformal, and energy autonomous all-nanofiber TENG–based e-skin with special functions such as high sensitivity, breathability, biodegradability, and antibacterial activity has been developed for the detection of physiological characteristics and movement states of the whole body. The all-nanofiber intercross network designed by sandwiching Ag NW electrode between the top PLGA triboelectric layer and the bottom PVA substrate contributes to the formation of a three-dimensional micro-to-nano porous hierarchical structure, which not only provides high specific surface area for contact electrification and pressure response but also ensures the thermal-moisture balance and wearing comfort of the surface skin microenvironment. Because of the biocidal property of Ag NWs, the e-skin shows remarkable antibacterial effect on *E. coli* and *S. aureus*. The service life of the e-skin can also be tuned from hours to weeks based on the selection and collocation of biodegradable PLGA and PVA. In addition, the e-skin based on the single electrode mode TENG has a maximum matching peak power density of 130 mW m^{-2} and a voltage response pressure sensitivity of 0.011 kPa^{-1}, which enables it to realize the whole-body physiological signal monitoring such as blinking, pulsing, speaking, and respiring, and major joint motion detections, including knuckle, elbow, knee, and ankle. On the basis of the merits of highly sensitive self-powered electrical responses, diversified practical functions, and remarkable human/environmental friendliness, the e-skin can assist the human body to navigate our physical world with ease. Although there are some aspects of the e-skin that need to be further optimized and improved, such as the asynchronous mechanical and degradation properties of its components, and the potential impact of humidity (e.g., human sweat) and pollutants, they can promote the research of e-skins to pay more attention to their practicability, such as comfortability, environmental friendliness, and antibacterial property while pursuing their high mechanical stability and high sensing sensitivity.

MATERIALS AND METHODS

Materials

PVA (M_w = 89,000 to 98,000; 99% hydrolyzed) was obtained from Sigma-Aldrich Chemical Co. Ltd. PLGA (75:25, M_w = 66,000 to 107,000) and hexafluoro-2-propanol (HFIP) were purchased form Aladdin Chemical Co. Ltd. Ag NW solution with an average diameter of 160 nm was provided by Nanjing XFNANO Materials Tech Co. Ltd. Deionized (DI) water was used in all of the experiments. All purchased chemicals were of analytical purity.

Fabrication of all-nanofiber e-skin

(i) Water-soluble PVA precursor was dissolved in DI water at concentrations ranging from 8 to 11 wt %, and then stirred for about 2 hours at 90°C. It was placed in a plastic syringe equipped with a 20-gauge metal needle. The collector covered with aluminum foil was placed 15 cm from the needle. The applied electric potentials ranging from 25 to 28 kV were applied by a high-voltage supply at the tip of the syringe needle. The PVA solution was subsequently electrospun at a constant flow rate. The electrospun PVA nanofibers were collected on aluminum foils positioned at a certain distance away from the injector nozzle. After electrospinning, PVA meshes were dried overnight under vacuum at room temperature to remove the residual water and then carefully peeled off from the aluminum foil. (ii) The PVA/Ag NW film was obtained by a vacuum filtration method. A piece of PVA nanofiber scaffold with the PET frame was used as a filtration film, and a diluted Ag NW dispersion was poured onto the PVA scaffold and vacuum filtrated by a sucking pump. A piece of copper foil was attached to the surface as the lead-out electrode. (iii) PLGA was dissolved in HFIP using a magnetic stirrer with concentrations ranging from 6.5 to 9.5 wt % for 12 hours. PLGA solution was fed into a plastic syringe fitted with a 23-gauge stainless steel blunt needle. The injection rate was adjusted from 0.3 to 1.0 ml/hour. High voltage (9 to 18 kV) was applied to the needle tip until a fluid jet was ejected. The aluminum foil covered with a PVA/Ag NW nanofiber film was used as the collector. The distance between the needle tip and the collector was fixed at 15 cm. The PLGA nanofiber scaffold was dried overnight under vacuum at room temperature.

Antibacterial test

The zone of inhibition is a clear area of interrupted growth underneath and along sides of the test material and indicates the bioactivity of the specimen on the basis of American Association of Textile Chemists and Colorists (AATCC 147). It is a qualitative test for the bacteriostatic activity by the diffusion of antibacterial agent through agar. The bacterial strains of gram-negative *E. coli* (CGMCC 1.8723) and gram-positive *S. aureus* (CGMCC 1.2155) used in this study were obtained from China General Microbiological Culture Collection Center (CGMCC). In particular, glassware, suction nozzles, and culture medium were sterilized in an autoclave at a high pressure of 0.1 MPa and a temperature of 120°C for 30 min before experiments. After cultivation in sterilized Luria-Bertani (LB) broth and then incubation at 37°C with a shaking incubator for 24 hours, both *E. coli* and *S. aureus* colonies were completely distributed on the empty agar plate (fig. S25). The concentration of bacterial suspensions was 10^8 colony-forming units (CFU)/ml throughout the antibacterial testing. The zone of inhibition method was performed

on the basis of the modified Kirby-Bauer method. The PVA, PLGA, and PLGA/Ag NWs/PVA nanofiber films were made into discs, with diameters of approximately 8 mm by using a hydraulic pressure and placed on the *E. coli* and *S. aureus* growth agar plates. The colony count method or the kinetic test was usually used to estimate antibacterial properties through the concentration of the survival colonies bacteria in cocultured solution. First, original bacterial suspensions were washed three times with phosphate-buffered saline (PBS; pH 7.4) solution to a concentration of 10^8 CFU/ml. Then, our samples were poured into the washed culture medium and incubated in a shaking bath for 1 hour. Third, the incubated solution was diluted five times to a certain concentration. The resulting bacterial PBS suspensions (100 μl) were spread on gelatinous LB agar plates, culturing at 37°C for 24 hours. The number of survival colonies was counted manually. The tests were repeated three times for each bacteria.

In vitro biodegradation test

Five types of nanofiber films were prepared for biodegradation tests, which are PVA, PLGA, Ag NWs/PVA, PVA/Ag NWs/PVA, and PLGA/Ag NWs/PVA. The dimensions of all the samples were fixed as 2 cm by 2 cm. Each sample was put in a 50-ml centrifuge tube, which was then filled with 30 ml of PBS (pH 7.4) solution. The PBS was autoclaved before use. Afterward, the tubes were placed in an incubator on a shaker table at 100 rpm at 37°C. The PBS buffer was refreshed weekly. To measure the weight change of samples for various periods (3, 10, 14, 21, 30, 40, and 50 days), samples were taken out from the PBS solution, then rinsed with DI water to remove the residual PBS solution, and dried in a vacuum oven at room temperature overnight. The weight loss in percentage was calculated according to a simple equation, i.e., weight loss (%) = $(W_0 - W_n)/W_0 \times 100$, where W_0 is the initial weight and W_n is the weight at a given degradation days.

Characterizations and measurements

The surface morphology and elemental component of the e-skin were characterized by field emission scanning electron microscope (Hitachi SU8020) equipped with EDX. The static water contact angle of the nanofiber films was performed by a contact angle analyzer (SL200B, Kino). The surface roughness of the e-skin was measured by AFM (Bruker, USA). The thermal stability of the nanofiber films was performed by thermogravimetric analysis (Pyris). XRD (Xper3 power) was used to characterize the crystalline structure of samples. An FTIR (VERTEX80v, Brucker) spectrometer was used to measure the infrared spectra of samples. Mechanical tensile behaviors were conducted using an ESM301/Mark-10 tester under a constant speed of 10 mm s^{-1}. The TENG-based e-skin was driven by a linear motor (Linmot E1100) for electrical measurement. A programmable electrometer (Keithley, model 6514) was used to test the open-circuit voltage, short-circuit current, and transferred charges. The software platform was constructed on the basis of LabVIEW. The applied force on the e-skin was measured by a compression dynamometer (Vernier LabQuest Mini). The thickness of the nanofiber film was measured by a thickness tester (CHY-CA, PARAM). The air permeability was measured by using an air permeability apparatus (YG461E, Wenzhou Fangyuan Instrument Co. Ltd., China) according to the ASTM D 737-75 standard test method under varied pressure drops.

SUPPLEMENTARY MATERIALS

Supplementary material for this article is available at http://advances.sciencemag.org/cgi/content/full/6/26/eaba9624/DC1

REFERENCES AND NOTES

1. X. Yu, Z. Xie, Y. Yu, J. Lee, A. Vazquez-Guardado, H. Luan, J. Ruban, X. Ning, A. Akhtar, D. Li, B. Ji, Y. Liu, R. Sun, J. Cao, Q. Huo, Y. Zhong, C. M. Lee, S. Y. Kim, P. Gutruf, C. Zhang, Y. Xue, Q. Guo, A. Chempakasseril, P. Tian, W. Lu, J. Y. Jeong, Y. J. Yu, J. Cornman, C. S. Tan, B. H. Kim, K. H. Lee, X. Feng, Y. Huang, J. A. Rogers, Skin-integrated wireless haptic interfaces for virtual and augmented reality. *Nature* **575**, 473–479 (2019).
2. S. Wang, J. Xu, W. Wang, G.-J. N. Wang, R. Rastak, F. Molina-Lopez, J. W. Chung, S. Niu, V. R. Feig, J. Lopez, T. Lei, S.-K. Kwon, Y. Kim, A. M. Foudeh, A. Ehrlich, A. Gasperini, Y. Yun, B. Murmann, J. B.-H. Tok, Z. Bao, Skin electronics from scalable fabrication of an intrinsically stretchable transistor array. *Nature* **555**, 83–88 (2018).
3. Z. Zou, C. Zhu, Y. Li, X. Lei, W. Zhang, J. Xiao, Rehealable, fully recyclable, and malleable electronic skin enabled bydynamic covalent thermoset nanocomposite. *Sci. Adv.* **4**, eaaq0508 (2018).
4. T. Q. Trung, N. E. Lee, Flexible and stretchable physical sensor integrated platforms for wearable human-activity monitoringand personal healthcare. *Adv. Mater.* **28**, 4338–4372 (2016).
5. X. Wang, Y. Gu, Z. Xiong, Z. Cui, T. Zhang, Silk-molded flexible, ultrasensitive, and highly stable electronic skin for monitoring human physiological signals. *Adv. Mater.* **26**, 1336–1342 (2014).
6. Y. Zhang, T. H. Tao, Skin-friendly electronics for acquiring human physiological signatures. *Adv. Mater.* **31**, e1905767 (2019).
7. K. Dong, Z. Wu, J. Deng, A. C. Wang, H. Zou, C. Chen, D. Hu, B. Gu, B. Sun, Z. L. Wang, A stretchable yarn embedded triboelectric nanogenerator as electronic skin for biomechanical energy harvesting and multifunctional pressure sensing. *Adv. Mater.* **30**, 1804944 (2018).
8. A. Chortos, J. Liu, Z. Bao, Pursuing prosthetic electronic skin. *Nat. Mater.* **15**, 937–950 (2016).
9. C. Wang, D. Hwang, Z. Yu, K. Takei, J. Park, T. Chen, B. Ma, A. Javey, User-interactive electronic skin for instantaneous pressure visualization. *Nat. Mater.* **12**, 899–904 (2013).
10. K. Dong, J. Deng, W. Ding, A. C. Wang, P. Wang, C. Cheng, Y.-C. Wang, L. Jin, B. Gu, B. Sun, Z. L. Wang, Versatile core-sheath yarn for sustainable biomechanical energy harvesting and real-time human-interactive sensing. *Adv. Energy Mater.* **8**, 1801114 (2018).
11. Y.-C. Lai, J. Deng, R. Liu, Y.-C. Hsiao, S. L. Zhang, W. Peng, H.-M. Wu, X. Wang, Z. L. Wang, Actively perceiving and responsive soft robots enabled by self-powered, highly extensible, and highly sensitive triboelectric proximity- and pressure-sensing skins. *Adv. Mater.* **30**, 1801114 (2018).
12. Y. Zang, F. Zhang, C.-a. Di, D. Zhu, Advances of flexible pressure sensors toward artificial intelligence and health care applications. *Mater. Horiz.* **2**, 140–156 (2015).
13. K. Dong, X. Peng, Z. L. Wang, Fiber/fabric-based piezoelectric and triboelectric nanogenerators for flexible/stretchable and wearable electronics and artificial intelligence. *Adv. Mater.* **32**, 1902549 (2019).
14. X. Wang, L. Dong, H. Zhang, R. Yu, C. Pan, Z. L. Wang, Recent progress in electronic skin. *Adv. Sci.* **2**, 1500169 (2015).
15. Y. Lee, J. Park, A. Choe, S. Cho, J. Kim, H. Ko, Mimicking human and biological skins for multifunctional skin electronics. *Adv. Funct. Mater.* **30**, 1904523 (2019).
16. Q. Hua, J. Sun, H. Liu, R. Bao, R. Yu, J. Zhai, C. Pan, Z. L. Wang, Skin-inspired highly stretchable and conformable matrix networks for multifunctional sensing. *Nat. Commun.* **9**, 244 (2018).
17. C. K. Jeong, S. B. Cho, J. H. Han, D. Y. Park, S. Yang, K.-I. Park, J. Ryu, H. Sohn, Y.-C. Chung, K. J. Lee, Flexible highly-effective energy harvester via crystallographic and computational control of nanointerfacial morphotropic piezoelectric thin film. *Nano Res.* **10**, 437–455 (2017).
18. C. Baek, J. H. Yun, J. E. Wang, C. K. Jeong, K. J. Lee, K.-I. Park, D. K. Kim, A flexible energy harvester based on a lead-free and piezoelectric BCTZ nanoparticle-polymer composite. *Nanoscale* **8**, 17632–17638 (2016).
19. Z. L. Wang, On the first principle theory of nanogenerators from Maxwell's equations. *Nano Energy* **68**, 104272 (2019).
20. K. Dong, J. Deng, Y. Zi, Y.-C. Wang, C. Xu, H. Zou, W. Ding, Y. Dai, B. Gu, B. Sun, Z. L. Wang, 3D orthogonal woven triboelectric nanogenerator for effective biomechanical energy harvesting and as self-powered active motion sensors. *Adv. Mater.* **29**, 1702648 (2017).
21. Z. L. Wang, A. C. Wang, On the origin of contact-electrification. *Mater. Today* **30**, 34–51 (2019).
22. K. Dong, Y.-C. Wang, J. Deng, Y. Dai, S. L. Zhang, H. Zou, B. Gu, B. Sun, Z. L. Wang, A highly stretchable and washable all-yarn-based self-charging knitting power textile composed of fiber triboelectric nanogenerators and supercapacitors. *ACS Nano* **11**, 9490–9499 (2017).
23. J. Wang, C. Wu, Y. Dai, Z. Zhao, A. Wang, T. Zhang, Z. L. Wang, Achieving ultrahigh triboelectric charge density for efficient energy harvesting. *Nat. Commun.* **8**, 88 (2017).
24. C. García Núñez, L. Manjakkal, R. Dahiya, Energy autonomous electronic skin. *npj Flexible Electronics* **3**, 1 (2019).

25. J. Wang, S. Li, F. Yi, Y. Zi, J. Lin, X. Wang, Y. Xu, Z. L. Wang, Sustainably powering wearable electronics solely by biomechanical energy. *Nat. Commun.* **7**, 12744 (2016).
26. H. S. Wang, C. K. Jeong, M.-H. Seo, D. J. Joe, J. H. Han, J.-B. Yoon, K. J. Lee, Performance-enhanced triboelectric nanogenerator enabled by wafer-scale nanogrates of multistep pattern downscaling. *Nano Energy* **35**, 415–423 (2017).
27. J. Deng, X. Kuang, R. Liu, W. Ding, A. C. Wang, Y.-C. Lai, K. Dong, Z. Wen, Y. Wang, L. Wang, H. J. Qi, T. Zhang, Z. L. Wang, Vitrimer elastomer-based jigsaw puzzle-like healable triboelectric nanogenerator for self-powered wearable electronics. *Adv. Mater.* **30**, 1705918 (2018).
28. R. Liu, X. Kuang, J. Deng, Y.-C. Wang, A. C. Wang, W. Ding, Y.-C. Lai, J. Chen, P. Wang, Z. Lin, H. J. Qi, B. Sun, Z. L. Wang, Shape memory polymers for body motion energy harvesting and self-powered mechanosensing. *Adv. Mater.* **30**, 1705195 (2018).
29. C. Larson, B. Peele, S. Li, S. Robinson, M. Totaro, L. Beccai, B. Mazzolai, R. Shepherd, Highly stretchable electroluminescent skin for optical signaling and tactile sensing. *Science* **351**, 1071–1074 (2016).
30. J. Park, Y. Lee, M. H. Barbee, S. Cho, S. Cho, R. Shanker, J. Kim, J. Myoung, M. P. Kim, C. Baig, S. L. Craig, H. Ko, A hierarchical nanoparticle-in-micropore architecture for enhanced mechanosensitivity and stretchability in mechanochromic electronic skins. *Adv. Mater.* **31**, e1808148 (2019).
31. M. Li, K. Chang, W. Zhong, C. Xiang, W. Wang, Q. Liu, K. Liu, Y. Wang, Z. Lu, D. Wang, A highly stretchable, breathable and thermoregulatory electronic skin based on the polyolefin elastomer nanofiber membrane. *Appl. Surf. Sci.* **486**, 249–256 (2019).
32. M. S. de Medeiros, D. Chanci, C. Moreno, D. Goswami, R. V. Martinez, Waterproof, breathable, and antibacterial self-powered e-textiles based on omniphobic triboelectric nanogenerators. *Adv. Funct. Mater.* **29**, 1904350 (2019).
33. M. Ma, Z. Zhang, Z. Zhao, Q. Liao, Z. Kang, F. Gao, X. Zhao, Y. Zhang, Self-powered flexible antibacterial tactile sensor based on triboelectric-piezoelectric-pyroelectric multi-effect coupling mechanism. *Nano Energy* **66**, 104105 (2019).
34. J. Tian, H. Feng, L. Yan, M. Yu, H. Ouyang, H. Li, W. Jiang, Y. Jin, G. Zhu, Z. Li, Z. L. Wang, A self-powered sterilization system with both instant and sustainable anti-bacterial ability. *Nano Energy* **36**, 241–249 (2017).
35. S. Wang, Q. Li, B. Wang, Y. Hou, T. Zhang, Recognition of different rough surface based highly sensitive silver nanowire-graphene flexible hydrogel skin. *Ind. Eng. Chem. Res.* **58**, 21553–21561 (2019).
36. R. Pan, W. Xuan, J. Chen, S. Dong, H. Jin, X. Wang, H. Li, J. Luo, Fully biodegradable triboelectric nanogenerators based on electrospun polylactic acid and nanostructured gelatin films. *Nano Energy* **45**, 193–202 (2018).
37. K. Parida, J. Xiong, X. Zhou, P. S. Lee, Progress on triboelectric nanogenerator with stretchability, self-healability and bio-compatibility. *Nano Energy* **59**, 237–257 (2019).
38. S. Wang, J. Y. Oh, J. Xu, H. Tran, Z. Bao, Skin-inspired electronics: An emerging paradigm. *Acc. Chem. Res.* **51**, 1033–1045 (2018).
39. S. Niu, S. Wang, L. Lin, Y. Liu, Y. S. Zhou, Y. Hu, Z. L. Wang, Theoretical study of contact-mode triboelectric nanogenerators as an effective power source. *Energy Environ. Sci.* **6**, 3576–3583 (2013).
40. Q. Zheng, Y. Zou, Y. Zhang, Z. Liu, B. Shi, X. Wang, Y. Jin, H. Ouyang, Z. Li, Z. L. Wang, Biodegradable triboelectric nanogenerator as a life-time designed implantable power source. *Sci. Adv.* **2**, e1501478 (2016).
41. H. Zou, Y. Zhang, L. Guo, P. Wang, X. He, G. Dai, H. Zheng, C. Chen, A. C. Wang, C. Xu, Z. L. Wang, Quantifying the triboelectric series. *Nat. Commun.* **10**, 1427 (2019).
42. Z. Zhang, Y. Wu, Z. Wang, X. Zhang, Y. Zhao, L. Sun, Electrospinning of Ag nanowires/polyvinyl alcohol hybrid nanofibers for their antibacterial properties. *Mater. Sci. Eng. C* **78**, 706–714 (2017).
43. C. Tang, W. Sun, J. Lu, W. Yan, Role of the anions in the hydrothermally formed silver nanowires and their antibacterial property. *J. Colloid Interface Sci.* **416**, 86–94 (2014).
44. H. K. Makadia, S. J. Siege, Poly lactic-co-glycolic acid (PLGA) as biodegradable controlled drug delivery carrier. *Polymers* **3**, 1377–1397 (2011).
45. C. A. Machado-Moreira, F. M. Smith, A. M. J. van den Heuvel, I. B. Mekjavic, N. A. S. Taylor, Sweat secretion from the torso during passively-induced and exercise-related hyperthermia. *Eur. J. Appl. Physiol.* **104**, 265–270 (2008).
46. Y. Khan, A. E. Ostfeld, C. M. Lochner, A. Pierre, A. C. Arias, Monitoring of vital signs with flexible and wearable medical devices. *Adv. Mater.* **28**, 4373–4395 (2016).
47. W. W. Nichols, Clinical measurement of arterial stiffness obtained from noninvasive pressure waveforms. *Am. J. Hypertens.* **18**, 3S–10S (2005).
48. C. Wang, X. Li, H. Hu, L. Zhang, Z. Huang, M. Lin, Z. Zhang, Z. Yin, B. Huang, H. Gong, S. Bhaskaran, Y. Gu, M. Makihata, Y. Guo, Y. Lei, Y. Chen, C. Wang, Y. Li, T. Zhang, Z. Chen, A. P. Pisano, L. Zhang, Q. Zhou, S. Xu, Monitoring of the central blood pressure waveform via a conformal ultrasonic device. *Nat. Biomed. Eng.* **2**, 687–695 (2018).
49. S. Lee, J. Kim, I. Yun, G. Y. Bae, D. Kim, S. Park, I.-M. Yi, W. Moon, Y. Chung, K. Cho, An ultrathin conformable vibration-responsive electronic skin for quantitative vocal recognition. *Nat. Commun.* **10**, 2468 (2019).

Acknowledgments

Funding: We are grateful for the support received from the Minister of Science and Technology (grant no. 2016YFA0202704) and the National Natural Science Foundation of China (grant nos. 61774016, 51432005, 5151101243, and 51561145021). No formal approval for the experiments involving human volunteers was required. The volunteers took part following informed consent. **Author contribution:** X.P., K.D., J.W., and Z.L.W. conceived the project and designed the e-skin. X.P., K.D., C.Y., Y.J., R.C., and D.L. fabricated the e-skin and designed and performed the experiments. X.P., K.D., and S.Z. conducted the antibacterial test. X.P., K.D., and X.G. conducted the air permeability test. X.P., K.D., J.W., and Z.L.W. analyzed the data and prepared the manuscript. All authors discussed the results and commented on the manuscript. **Competing interests:** X.P., K D., J.W., and Z.L.W. are inventors on a patent related to this work that is currently under review with the State Intellectual Property Office of P. R. China (serial no. 202010333458.4, 26 April 2020). The other authors declare that they have no conflict of interest. **Data and materials availability:** All data needed to evaluate the conclusions in the paper are present in the paper and/or the Supplementary Materials. Additional data related to this paper may be requested from the authors.

Submitted 19 January 2020
Accepted 15 May 2020
Published 26 June 2020
10.1126/sciadv.aba9624

Citation: X. Peng, K. Dong, C. Ye, Y. Jiang, S. Zhai, R. Cheng, D. Liu, X. Gao, J. Wang, Z. L. Wang, A breathable, biodegradable, antibacterial, and self-powered electronic skin based on all-nanofiber triboelectric nanogenerators. *Sci. Adv.* **6**, eaba9624 (2020).

Science Advances

A breathable, biodegradable, antibacterial, and self-powered electronic skin based on all-nanofiber triboelectric nanogenerators

Xiao Peng, Kai Dong, Cuiying Ye, Yang Jiang, Siyuan Zhai, Renwei Cheng, Di Liu, Xiaoping Gao, Jie Wang and Zhong Lin Wang

Sci Adv **6** (26), eaba9624.
DOI: 10.1126/sciadv.aba9624